Volume 1 | Number 1 | Jan 2013 | Pages 1–100

ChemComm

Chemical Communications
www.rsc.org/chemcomm

ROYAL SOCIETY OF CHEMISTRY

ROYAL SOCIETY OF CHEMISTRY

www.rsc.org/chemcomm

Please do not adjust margins

ChemComm

Journal Name

COMMUNICATION

Plasmonic MoO₃₋ₓ@MoO₃ Nanosheets for Highly Sensitive SERS Detection through Nanoshell-Isolated Electromagnetic Enhancing

Xianjun Tan,[a] Lingzhi Wang,[a]* Chen Cheng,[a] Xuefeng Yan,[a] Bin Shen[a] and Jinlong Zhang[a]*

Plasmonic MoO₃₋ₓ@MoO₃ nanosheets obtained from surface oxidation of MoO₃₋ₓ were employed as SERS substrate for the detection of methylene blue. They exhibit extraordinary sensitivity comparable to noble metals, which is attributed to the shell-isolated electromagnetic enhancing by plasmonic MoO₃₋ₓ core and elimination of photocatalytic degradation by MoO₃ shell.

Localized surface plasmon resonance (LSPR) in noble metal nanostructures (Au, Ag, Cu) has long been a subject of intense research due to their special optical property and potential applications in a variety of scientific disciplines.[1] Recently, it has been discovered that heavily self-doped semiconductor with sufficient free carrier density such as TiO_{2-x}, $Cu_{2-x}S$, WO_{3-x} and $Cu_{2-x}Te$ also exhibit metal-like LSPR,[2] which stimulates a research upsurge of plasmonic nanomaterials beyond the traditional coinage metals. Most LSPRs of plasmonic semiconductors locate in the long-wavelength range of near-infrared (NIR) and even middle-infrared (MIR). Fortunately, it has been recently found that the wavelength can be tuned to the short-wavelength range of NIR (780-1100 nm). These plasmonic semiconductors with LSPR frequency comparable to noble metals are expected to substitute or complement the noble metals in a wide range of photonic applications.[3]

In the context of surface-enhanced Raman scattering (SERS) detection, noble nanostructures have been extensively studied and applied to the molecular analysis in the fields of environment, catalysis and biology.[4] Alternatively, semiconductors, when employed as SERS substrate, can provide an extensive insight into the binding conformation of adsorbed molecules, sorption geometry and interfacial information,[5] which however has long been ignored due to the low sensitivity. Plasmonic semiconductors with LSPR wavelength located in the short-wavelength range of NIR is

expected to gain comparable SERS activity to noble metals.[6] It is known that plasmonic semiconductors exhibit similar size- and shape-tunability of LSPRs as metals.[6] The difference lies in that the LSPR of semiconductor that is dependent on the free carrier concentration is variable with doping, temperature or phase transitions, while the LSPR of metal nanocrystals with specified shape or size can not be engineered due to the fixed carrier density.[7] Currently, the relationship between the fundamental features of electronic structure (eg. carrier density and distribution) and SERS activity of plasmonic semicondctor has been poorly understood. Question about whether plasomic semiconductor has SERS characteristics resembling that of metals still remains ambiguous, which requires great effort to explore the acurate enhancing mechanism and finally achieve high detection sensitivity.

In this work, plasmonic MoO₃₋ₓ nanosheets with various LSPR frequencies and intensities from visible to NIR region were employed to the SERS detection of methylene blue (MB), which show unusual activity opposite to the plasmonic resonance intensity. In comparison, the nanosheets after a mild annealing treatment at 200 °C show noteworthy sensitivity to MB with an high enhanced factor (EF) of 1.42 ×

a. Key Laboratory for Advanced Materials and Institute of Fine chemicals, East China University of Science and Technology, Shanghai 200237, P.R. China.
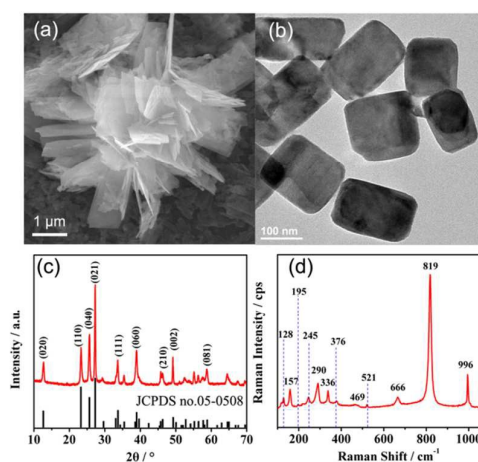Email: wlz@ecust.edu.cn; jlzhang@ecust.edu.cn.

Fig. 1 (a) SEM image, (b) TEM image, (c) XRD pattern and (d) Raman spectrum of MoO₃₋ₓ nanosheets prepared at 170 °C.

10^5 and extremely low dectection limit of 10^{-7} M. Core-shell structured $MoO_{3-x}@MoO_3$ nanosheets were formed after the calcination process, which are composed of plasmonic MoO_{3-x} core due to preserved free carrier density of 5.3×10^{21} cm^{-3} in the bulk and non-plasmonic MoO_3 shell. The photocatalytic degradation of analyte is revealed to be responsible for the low SERS activity of naked MoO_{3-x} nanosheets. In contrast, high sensitivity can be achieved on $MoO_{3-x}@MoO_3$ through shell-isolated electromagnetic enhancing by plasmonic MoO_{3-x} core and the elimination of photocatalytic degradation on MoO_3 shell. To our best knowledge, this is the first time to unambiguously elaborate the SERS enhancing mechanism of plasmonic semiconductors.

MoO_{3-x} nanosheets were synthesized by a solvothermal procedure, in which methanol as solvent and reducing agent was introduced into the molybdenum precursor solution (see in SI).[8] Scanning electron microscopy (SEM) indicates a flower-like structure stacked from nanosheets with a thickness of 20-30 nm (Fig. 1a). Atomic force microscopy (AFM) confirms the mean thickness of the nanosheets to be 28.7 nm (Fig. S1). Transmission electron microscopy (TEM) shows that the as-prepared MoO_{3-x} nanosheets exhibit a rectangle shape with an average length and width of 80-200 nm (Fig. 1b). X-ray diffraction (XRD) pattern in Fig. 1c reveals sharp peaks attributed to the orthorhombic structure, which is the same as that of MoO_3 (JCPDS no.05-0508). Raman spectrum also presents characteristic peaks of orthorhombic phase.[9] Typically, the peak at 996 cm^{-1} represents the stretching mode of the terminal oxygen (Mo=O) vibration. The peak at 819 cm^{-1} is assigned to the doubly coordinated oxygen (Mo$_2$-O) stretching mode. The peak at 290 cm^{-1} is ascribed to the bending mode for double bond (Mo=O) vibration (Fig. 1d).[10]

The optical property of the MoO_{3-x} nanosheets was further investigated by UV-Vis-NIR diffuse reflectance spectroscopy (Fig. 2a). The nanosheets prepared at 170 °C (MoO_{3-x}-170 °C) exhibit a broad absorption band centered at approximately 950 nm in the visible and NIR region. The absorption is associated with LSPR due to the existence of substantial free carrier. The absorption peak shows bathochromic shift (λ_{max} =

750 nm) when the reaction temperature increases to 180 °C, accompanied by an improved resonance intensity. The UV-vis-NIR absorption spectroscopy also displays in Fig. S2. It also shows a broad absorption band from visible to NIR region. The free carrier density (N) is calculatd according to the Drude model

$$\omega_p = \sqrt{\frac{Ne^2}{\varepsilon_0 m_e}} \qquad (1)$$

where ω_p is the bulk plasmon frenquency, e is the elementary charge, ε_0 is the permittivity of free space, and the effective mass of the free carrier m_e is assumed to be that of a free electron.[2c, 7e] The charge carrier densities are determined to be 5.3×10^{21} and 8.1×10^{21} cm^{-3} for the sample MoO_{3-x}-170 °C and MoO_{3-x}-180 °C (see in S3), respectively. The products MoO_{3-x}-170 °C and MoO_{3-x}-180 °C exhibit characteristic blue and intense blue colours due to the existence of outer-d electrons arising from the intervalence charge-transfer between Mo^{5+} and Mo^{6+} in MoO_{3-x} (Fig. 2b).[11] In comparison, the commercial MoO_3 presents a light kelly color with only a slight 'tail' absorption beyond 400 nm. Electron paramagnetic resonance (EPR) and X-ray photoelectron spectroscopy (XPS) techniques were further performed to elucidate the electronic property of the MoO_{3-x} nanosheets. As shown in Fig. 2c, three distinct peaks at $g_x = 1.999$, $g_y = 1.936$, $g_z = 1.874$ are observed in plasmonic MoO_{3-x} nanosheets, which can be attributed to paramagnetic Mo^{5+} centers.[12] In contrast, commercial MoO_3 shows negligible peak corresponding to Mo^{5+}. The Mo 3d XPS spectrum of sample MoO_{3-x}-170 °C shows two peaks which can be fitted into doublets (Fig. 2d). The characteristic peaks at 235.8 and 232.6 eV are assigned to Mo^{6+}, and the peaks at 235.0 and 231.9 eV correspond to Mo^{5+}.[8a, 11] The binding energies of sample MoO_{3-x}-180 °C further shift to the lower position. These results are in good agreement with the optical analysis, proving the presence of free electrons which can localize to form Mo^{5+} centers and oxygen vacancies.

It is known that noble metals have been widely employed as SERS-active substrates due to their intense LSPR absorption in visible region, which can improve the electromagnetic field and produce high Raman intensity by factors of 10^6 to 10^{12}. The strong LSPR absorption of MoO_{3-x} nanosheets spanning from the visible to NIR region allows us to explore the potential application of plasmonic MoO_{3-x} semiconductor in SERS detection. Here, MB was adopted as the model analyte. For SERS measurement, 5 mg sample was ultrasonically dispersed in the MB ethanol solution (1 mL), and 20 μL of the mixture was then transferred on a silica wafer. Raman spectra were recorded using a 50X objective and 785 nm laser excitation with 0.5 mW incident power. It is surprisingly found that the SERS activity of plasmonic MoO_{3-x} is lower than the non-plasmonic commercial MoO_3 (Fig. 3a). The Raman signal of MB even even decreases with the increasing LSPR field, where only a faint Raman signal can be observed from MoO_{3-x}-180 °C. This result is extremely abnormal but interesting compared to noble metals. Moreover, it is notable that plasmonic MoO_{3-x} exhibit better photocatalytic activity towards MB than the commercial MoO_3 under visible light
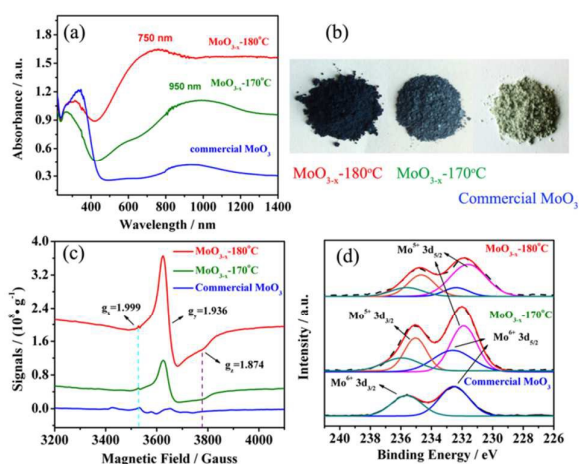

Fig. 2 (a) UV-Vis-NIR diffuse reflectance, (b) Optical photograph, (c) EPR spectra and (d) Mo 3d XPS spectra of plasmonic MoO_{3-x} nanosheets and commercial MoO_3.
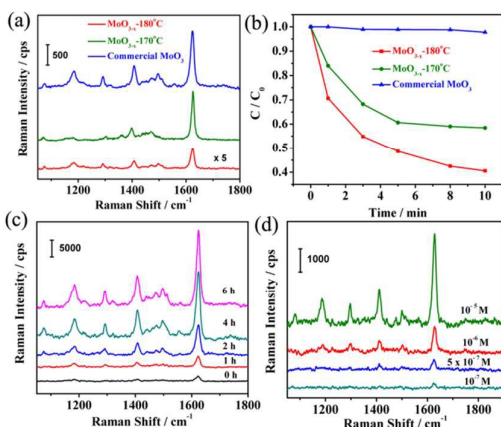
COMMUNICATION

Fig. 3 (a) SERS spectra of MB (10^{-4} M) adsorbed on plasmonic MoO_{3-x} and commercial MoO_3; (b) Photocatalytic degradation of MB on plasmonic MoO_{3-x} and commercial MoO_3; (c) SERS spectra of MB (10^{-4} M) on plasmonic MoO_{3-x}-170 ^oC calcined at 200 ^oC for different times; (d) SERS spectra of MB collected for MoO_{3-x} nanosheets after calciation at 200 ^oC for 6 h at different concentrations.

irradiation (Fig. 3b) and the activity is proportional to the LSPR intensity. It is acknowledged that the exsitense of reductive metal ceters and oxygen vancencies can supress recombination of photogenerated electons and holes and improve the photocatalytic efficiency, suggesting the photocatalytic degradation should be related to the decreased SERS activity.

In addition, we further unexpectedly found that higher Raman signal can be observed from the sample preserved in an aerobic environment for about 1 week. It is known the surface Mo^{5+} tends to be oxidized to Mo^{6+}, indicating the distribution of free carrier may influence the SERS activity of plasmonic MoO_{3-x}. To clarify the relationship between the distribution of free carrier and SERS activity, the plasmonic MoO_{3-x} nanosheets were mildly annealed at 200 ^oC for different times to eliminate the surface Mo^{5+} species and oxygen vacancies. As demonstrated in Fig. 3c, the Raman signals of MB (10^{-4} M) gradually enhance with the increasing calcination time from 0 to 4 h, which then keep stable as the calcination time is further prolonged to 6 h. The intensity is almost 10-fold improved compared to that on non-plasmonic MoO_3 as calculated from the peak intensity at 1625 cm^{-1}. The detection limit is low to 10^{-7} M (Fig. 3d), which is hard to be achieved on semiconductor substrates. The enhanced factor (EF) is calculated to be 1.42×10^5 (Fig. S3), comparable to those observed from noble metals.

Furthermore, analysis about the LSPR characteristics of the calcined samples indicates the LSPR frequency maintain almost unchanged after calcination treatment, while the intensity decreases with the prolonging calcination time from 0 to 4 h and keeps stable even after 20 h of calcination (Fig. 4a), which suggest the free carrier density of the calcined samples in the bulk has not been changed after the calcination treatment. To get insight into the reason for the decreased LSPR intensity, EPR and XPS techniques were further used to analyze the structure characteristics of the calcined samples. Fig. 4b indicates the EPR of the sample annealed for 1 h shows a
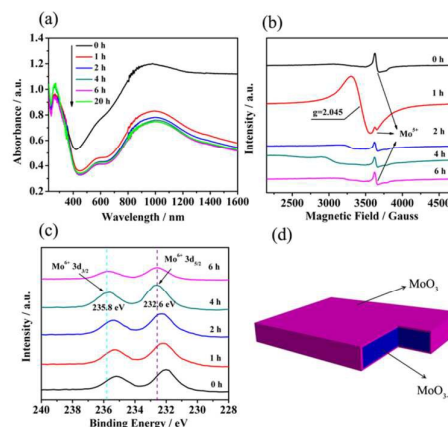

Fig. 4 (a) UV-vis-NIR diffuse reflectance, (b) EPR and (c) Mo 3d XPS spectra of MoO_{3-x} nanosheets after calcination at 200 ^oC. (d) Shematic diagram of the MoO_{3-x}@MoO_3 nanosheets.

broad peak at g = 2.045. It is known that the reductive metal center or oxygen vacancy has strong affinity to moelcule O_2,[13] forming metal ion-O_2^- complex on the surface of reduced metal oxide. Therefore, the signal should be attributed to Mo^{6+}-O_2^- transformed from Mo^{5+}-O_2 during the thermal treatment process. The amount of surface Mo^{5+} in the nanosheets decreases with the increasing calcination time, leading to the gradual vanishing of this signal. XPS also confirms that Mo^{5+} species decreases with the increasing calcination time (Fig. 4c). After calcination for 6 h, Mo^{5+} species on the surface of the plasmonic MoO_{3-x} nanosheets completely transforms into Mo^{6+}. Moreover, the photoluminescence (PL) intensity becomes stronger with the extended calcination time, implying the simultaneous elimination of surface oxygen vacancy with strong capability to capture the excited electrons (Fig. S4). Since XPS is a surface analysis technique with the detection depth of ca. 2-3 nm, core-shell structured MoO_{3-x}@MoO_3 nanosheets composed of plasmonic MoO_{3-x} core with preserved free carrier concentration (5.3×10^{21} cm^{-3}) and non-plasmonic MoO_3 shell should be formed after the mild calcination treatment according to the unvaried free carrier density and eliminated surficial Mo^{5+} and oxygen vacancy (Fig. 4d).

Additionally, in order to rule out the possible influence of morphological change by calcination on SERS ananlysis, the calcined sample was further characterized by TEM (Fig. S5). It is observed that the calcined sample keeps the original structure without apparant aggregation. To avoid the detection occasionality, the Raman measurements were totally recorded for 20 times. The RSD was calculated to be 8.6%, which confirms the good reproducibility of the nanosheets as SERS substrate (Fig. S6). Moreover, Raman intensity should depend on the volume of MoO_{3-x} within the surface oxidized nanosheets and from the MoO_{3-x} core and the MB adsorbed on the surface. To further invesigate this point, the nanosheets were calcined at higher tempratures of 300 ^oC and 500 ^oC for 6 h. The maximum absorption wavelength of the sample calcined at 300 ^oC almost keeps the same as that calcined at 200 ^oC, indicating the free carrier density is not changed at this

temperature (Fig. S7a). However, the intensity is observably decreased, which should be attributed to the further improved shell thickness. Meanwhile, the sample calcined at 500 ^{o}C completely loses the plasmonic characteristic according to the disappeared absorption peak. Accordingly, the SERS activity decreases with increasing calcination temperature above 200 ^{o}C, owing to the decrease of LSPR field and improved distance between MB and MoO_{3-x} core (Fig. S7b).

Based on the above results, a possible shell-isolated electromagnetic enhancing mechanism was proposed to elucidate the essence of SERS activation on $MoO_{3-x}@MoO_3$. As illustrated in Scheme 1, for the plasmonic MoO_{3-x} nanosheets, the presense of defective sites (Mo^{5+} centers and oxygen vacancies) may produce a new band below the bottom of original conduction band, which decreases recombination of the photogenerated electrons and holes, as verified by the PL spectra metioned above. Therefore, the charge transfer and separation in MoO_{3-x} can be effetively promoted and degradation efficency is further improved. On the other hand, the Mo^{5+} species and oxygen vacancies on the surface of plasmonic MoO_{3-x} has strong affinity to atmospheric O_2. The surface should be preferentially covered by O_2, producing photocatalytically active $\cdot O_2^-$ species under laser irradiation. Therefore, MB may be locally degraded during the detection process, leading to the low SERS activity of plasmonic MoO_{3-x}. However, for plasmonic $MoO_{3-x}@MoO_3$, the elimination of the Mo^{5+} centers and oxygen vacancies make the photocatalytic degradation of MB unacheviable because of the stoichiometric MoO_3 shell after calcianation treatment. In this case, the shell-isolated electromagnetic enhancing by plasmonic MoO_{3-x} core finally leads to the extraordinary detection sensitivity comparable to that of noble metals.

In summary, the SERS activity of plasmonic MoO_{3-x} nanosheets is revealed to be inversely proportional to the LSPR intensity. In contrast, extraordinary sensitivity can be achieved on core-shell $MoO_{3-x}@MoO_3$ obtained from surface oxidation of MoO_{3-x}, which is attributed to the shell-isolated electromagnetic enhancing by plasmonic MoO_{3-x} core with preserved free carrier concentration and the elimination of photocatalytic degradation by MoO_3 shell. These findings pave the way for deeply understanding the enhancement mechanism of emerging plasmonic semiconductors in SERS analysis and would further promote their tremendous potential application concerned with LSPR.
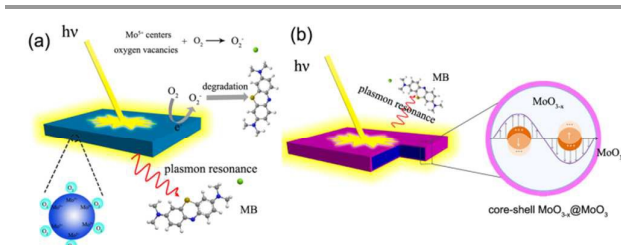
Scheme 1. Proposed mechanism for SERS enhancement depending on nanoshell-isolated electromagnetic enhancing mechanism for plasmonic $MoO_{3-x}@MoO_3$ nanosheets.

Notes and references

1   (a) M. R. Jones, K. D. Osberg, R. J. Macfarlane, M. R. Langille and C. A. Mirkin, *Chem. Rev.*, 2011, **111**, 3736; (b) K. M. Mayer and J. H. Hafner, *Chem. Rev.*, 2011, **111**, 3828.
2   (a) T. R. Gordon, M. Cargnello, T. Paik, F. Mangolini, R. T. Weber, P. Fornasiero and C. B. Murray, *J. Am. Chem. Soc.*, 2012, **134**, 6751; (b) Y. Zhao, H. Pan, Y. Lou, X. Qiu, J. Zhu and C. Burda, *J. Am. Chem. Soc.*, 2009, **131**, 4253; (c) K. Manthiram and A. P. Alivisatos, *J. Am. Chem. Soc.*, 2012, **134**, 3995; (d) A. M. Schimpf, S. D. Lounis, E. L. Runnerstrom, D. J. Milliron and D. R. Gamelin, *J. Am. Chem. Soc.*, 2015, **137**, 518; (e) I. Kriegel, J. Rodríguez-Fernández, A. Wisnet, H. Zhang, C. Waurisch, A. Eychmüller, A. Dubavik, A. O. Govorov and J. Feldmann, *ACS Nano*, 2013, **7**, 4367; (f) S. W. Hsu, W. Bryks and A. R. Tao, *Chem. Mater.*, 2012, **24**, 3765.
3   (a) X. Wang, Y. Ke, H. Pan, K. Ma, Q. Xiao, D. Yin, G. Wu and M. T. Swihart, *ACS Catal.*, 2015, **5**, 2534; (b) X. Ding, C. H. Liow, M. Zhang, R. Huang, C. Li, H. Shen, M. Liu, Y. Zou, N. Gao, Z. Zhang, Y. Li, Q. Wang, S. Li and J. Jiang, *J. Am. Chem. Soc.*, 2014, **136**, 15684; (c) A. Llordes, G. Garcia, J. Gazquez and D. J. Milliron, *Nature*, 2013, **500**, 323; (d) S. Wang, A. Riedinger, H. Li, C. Fu, H. Liu, L. Li, T. Liu, L. Tan, M. J. Barthel, G. Pugliese, F. De Donato, M. Scotto D'Abbusco, X. Meng, L. Manna, H. Meng and T. Pellegrino, *ACS Nano*, 2015, **9**, 1788.
4   (a) S. Nie and S. R. Emory, *Science*, 1997, **275**, 1102; (b) J. F. Li, Y. F. Huang, Y. Ding, Z. L. Yang, S. B. Li, X. S. Zhou, F. R. Fan, W. Zhang, Z. Y. Zhou and B. Ren, *nature*, 2010, **464**, 392; (c) J. A. Dieringer, K. L. Wustholz, D. J. Masiello, J. P. Camden, S. L. Kleinman, G. C. Schatz and R. P. Van Duyne, *J. Am. Chem. Soc.*, 2009, **131**, 849; (d) Y. Wang, B. Yan and L. Chen, *Chem. Rev.*, 2012, **113**, 1391.
5   (a) I. Urdaneta, A. Keller, O. Atabek, J. L. Palma, D. Finkelstein-Shapiro, P. Tarakeshwar, V. Mujica and M. Calatayud, *J. Phys. Chem. C*, 2014, **118**, 20688; (b) N. Lee, P. J. Schuck, P. S. Nico and B. Gilbert, *J. Phys. Chem. Lett.*, 2015, **6**, 970.
6   W. Li, R. Zamani, P. Rivera Gil, B. Pelaz, M. Ibanez, D. Cadavid, A. Shavel, R. A. Alvarez-Puebla, W. J. Parak, J. Arbiol and A. Cabot, *J. Am. Chem. Soc.*, 2013, **135**, 7098.
7   (a) A. Comin and L. Manna, *Chem. Soc. Rev.*, 2014, **43**, 3957; (b) J. A. Faucheaux, A. L. D. Stanton and P. K. Jain, *J. Phys. Chem. Lett.*, 2014, **5**, 976; (c) X. Liu and M. T. Swihart, *Chem. Soc. Rev.*, 2014, **43**, 3908; (d) S. D. Lounis, E. L. Runnerstrom, A. Llordés and D. J. Milliron, *J. Phys. Chem. Lett.*, 2014, **5**, 1564; (e) J. M. Luther, P. K. Jain, T. Ewers and A. P. Alivisatos, *Nat. Mater*, 2011, **10**, 361.
8   (a) H. Cheng, T. Kamegawa, K. Mori and H. Yamashita, *Angew. Chem. Int. Ed.*, 2014, **53**, 2910; (b) G. Song, J. Shen, F. Jiang, R. Hu, W. Li, L. An, R. Zou, Z. Chen, Z. Qin and J. Hu, *ACS Appl. Mater. Interfaces*, 2014, **6**, 3915.
9   (a) R. Liang, H. Cao and D. Qian, *Chem. Commun.*, 2011, **47**, 10305; (b) L. Q. Mai, B. Hu, W. Chen, Y. Y. Qi, C. S. Lao, R. S. Yang, Y. Dai and Z. L. Wang, *Adv. Mater.*, 2007, **19**, 3712.
10 J. Z. Ou, J. L. Campbell, D. Yao, W. Wlodarski and K. Kalantar-zadeh, *J. Phys. Chem. C*, 2011, **115**, 10757.
11 Q. Huang, S. Hu, J. Zhuang and X. Wang, *Chem. Eur. J.*, 2012, **18**, 15283.
12 (a) R. B. Watson and U. S. Ozkan, *J. Phys. Chem. B*, 2002, **106**, 6930; (b) V. Hornebecq, Y. Mastai, M. Antonietti and S. Polarz, *Chem. Mater.*, 2003, **15**, 3586; (c) J. Xiong, Y. Liu, D. Wang, S. Liang, W. Wu and L. Wu, *J. Mater. Chem. A*, 2015, **3**, 12631.
13 (a) S. Tan, Y. Ji, Y. Zhao, A. Zhao, B. Wang, J. Yang and J. G. Hou, *J. Am. Chem. Soc.*, 2011, **133**, 2002; (b) U. Aschauer, J. Chen and A. Selloni, *Phys. Chem. Chem. Phys.*, 2010, **12**, 12956; (c) F. Zuo, L. Wang, T. Wu, Z. Zhang, D. Borchardt and P. Feng, *J. Am. Chem. Soc.*, 2010, **132**, 11856.